polymers

MDPI

Article

Effect of UV-C Radiation on 3D Printed ABS-PC Polymers

Catalin Gheorghe Amza *, Aurelian Zapciu, Florin Baciu and Constantin Radu

Faculty of Industrial Engineering and Robotics, University Politehnica of Bucharest, 060042 Bucharest, Romania; aurelianzapciu@yahoo.com (A.Z.); florin.baciu@upb.ro (F.B.); rcdnd@yahoo.com (C.R.)
* Correspondence: acata1@camis.pub.ro; Tel.: +40-744-500-803

Abstract: During the initial stages of the COVID-19 pandemic, healthcare facilities experienced severe shortages of personal protective equipment (PPE) and other medical supplies. Employing 3D printing to rapidly fabricate functional parts and equipment was one of the emergency solutions used to tackle these shortages. Using ultraviolet light in the UV-C band (wavelengths of 200 nm to 280 nm) might prove useful in sterilizing 3D printed parts, enabling their reusability. Most polymers, however, degrade under UV-C radiation, so it becomes necessary to determine what 3D printing materials can withstand the conditions found during medical equipment sterilization with UV-C. This paper analyzes the effect of accelerated aging through prolonged exposure to UV-C on the mechanical properties of parts 3D printed from a polycarbonate and acrylonitrile butadiene styrene polymer (ABS-PC). Samples 3D printed using a material extrusion process (MEX) went through a 24-h UV-C exposure aging cycle and then were tested versus a control group for changes in tensile strength, compressive strength and some selected material creep characteristics. Testing showed minimal mechanical property degradation following the irradiation procedure, with tensile strength being statistically the same for irradiated parts as those in the control group. Irradiated parts showed small losses in stiffness (5.2%) and compressive strength (6.5%). Scanning electron microscopy (SEM) was employed in order to assess if any changes occurred in the material structure.

Keywords: 3D-printing polymers; ABS-PC; PCABS; accelerated aging; ultraviolet; UV-C

Citation: Amza, C.G.; Zapciu, A.; Baciu, F.; Radu, C. Effect of UV-C Radiation on 3D Printed ABS-PC Polymers. *Polymers* **2023**, *15*, 1966. https://doi.org/10.3390/polym15081966

Academic Editors: Cristina-Elisabeta Pelin and Anton Ficai

Received: 30 March 2023
Revised: 13 April 2023
Accepted: 19 April 2023
Published: 21 April 2023

1. Introduction

In the early weeks of the COVID-19 pandemic, healthcare facilities were overwhelmed by the influx of people requiring medical assistance, leading to problems with personal protective equipment supply and availability, as stated by the World Health Organization [1]. These shortages were widespread and happened at all levels of medical care, from nursing homes, local hospitals and clinics to emergency rooms at some of the world's biggest hospitals [2–4]. The distribution of locations that needed equipment and the diversity of items needed made resupplying extremely difficult, both from a manufacturing perspective and from a logistical one [5–8]. The necessary equipment had to be manufactured quickly and had to be distributed widely, which led to even more problems occurring because of resource misallocation [9,10]. Additive manufacturing (AM), also known as 3D printing, has a decentralized aspect and a unique ability to adapt to producing new part designs without additional capital investment [11–14]. With AM, parts can be produced on-site and on-demand, lowering the delay between necessity and availability. For this reason, 3D printing saw increased use during the initial responses to the medical equipment shortages [15–17]. Hospital technicians, small businesses and even private citizens who owned hobby-grade 3D printers began creating, distributing and manufacturing designs of protective equipment [18–20].

While the majority of the manufactured products meant to replace medical equipment in case of critical and urgent supply issues were designed for single use (e.g., swabs for nasopharyngeal testing [21–23]), other products could be used multiple times if sterilized under inadequate conditions. Examples of such products are face shields [24,25].

Material Extrusion 3D Printing (MEX) is an additive manufacturing process [26] that uses thermoplastic material feedstock. MEX 3D printing enables several advantages over more traditional manufacturing.

Studies performed on N95 respirators during the COVID-19 pandemic showed that filtering efficiency and infection prevention increase when the respirator is properly fitted [27–29]. The fact that 3D printing can be used to rapidly manufacture bespoke products for each healthcare worker can be leveraged to provide better and tighter seals for respirators. Ballard et al. produced respirators using real 3D data obtained using computer tomography that successfully passed OSHA-certified testing [30], while McAvoy et al. produced polymer frames that improve the fit of available N95 respirators [31].

In the medical field, the sterilization of medical equipment is performed through various methods, such as autoclaving, dry heating, ultrasonic sterilization [32–35], or chemical sterilization using various chemicals, such as hydrogen peroxide or ethylene oxide [36]. However, some of these methods are not applicable to certain polymers. For example, acrylonitrile butadiene styrene (ABS) parts deform when going through repeated autoclaving treatments [37] and suffer from a degradation of mechanical properties when sterilized using alcohol or other disinfectants [38,39].

In recent years, researchers have paid increasing attention to the sterilizing action of ultraviolet radiation, specifically UV-C radiation [40–43]. The International Commission on Illumination (in French: Commission Internationale de l'Eclairage, CIE) uses a wavelength of 280 nm to separate UV-C and UV-B bands, 315 nm to separate UV-B and UV-A bands, and 400 nm to separate UV-A and photosynthetically active radiation. The effects of UV-B/UV-A radiation have been studied extensively, as radiation of these wavelengths reaches Earth's troposphere naturally. However, UV-C radiation is entirely filtered by the Earth's atmosphere and has to be produced artificially. For this reason, there is no accelerated aging testing standard for the action of UV-C on materials, unlike that for radiation of longer wavelengths [44]. A workshop organized by the United States National Institute of Standards and Technology (NIST) and the International UV Association (IUVA) [45] aimed to gather information about applications, new certifications and new guidelines regarding UV-C disinfection and sterilization [46]. This workshop also highlighted the need to study the effects of UV-C radiation on materials. Standards for UV-C applications and testing are currently under development as a cooperation between NIST and the Illuminating Engineering Society (IES.org).

To get ahead of this trend, materials testing is important in determining their applicability and compatibility with novel sterilization methods. In the case of UV-C sterilization, materials testing is also crucial to the standardization efforts.

Acrylonitrile Butadiene Styrene (ABS) is a 3D printing material with widespread use [47] due to its good mechanical characteristics [48,49] and low cost. The material is known for its weak ultraviolet resistance [50]. Through the addition of polycarbonate fibers (PC) to an ABS base, manufacturers have successfully created a copolymer blend with enhanced mechanical properties and ultraviolet resistance [51] while still maintaining its ease of processing through MEX 3D printing [52]. This copolymer has high strength and stiffness, high heat resistance [53,54], and good impact resistance [55]. The newly created acrylonitrile butadiene styrene and polycarbonate polymer blends (ABS-PC) are being marketed for use in industrial applications, prototyping, toolmaking or end-use parts manufacturing [56].

Given this context, this work investigates the changes in the mechanical behavior of 3D-printed parts made from ABS-PC after exposure to artificial UV-C radiation. This work pursues one of the research directions raised by the NIST-IUVA workshop highlighted previously related to identifying and studying suitable materials. Unlike more common polymers, such as ABS, polylactic acid (PLA), or modified polyethylene terephthalate-glycol (PETG), literature on 3D printed ABS-PC blends is scarce and does not include mechanical behavior after exposure to artificial radiation in the UV-C spectrum. Additionally, the study of 3D printed materials is necessary for the implementation and approval of 3D

printing techniques and 3D printed devices for medical applications, including those produced at the point of care (3DPOC) [57,58]. By using a controlled irradiation treatment in an irradiation chamber, an accelerated effect that simulates many cycles of ultraviolet sterilization can be observed. The mechanical properties assessed in this work are tensile and compression strength, material stiffness, as well as changes in creep behavior of ABS-PC samples subjected to prolonged tensile loads.

2. Materials and Methods

Accelerated aging of materials under UV-C radiation does not have well-defined testing standards. Testing parameters and procedures should be determined based on existing literature. An appendix of the ISO 4892-2 standard [59] mentions modifying testing conditions to use a mercury lamp that generates 10 W/m^2 of 254 nm wavelength radiation, a wavelength that falls in the UV-C band. A testing protocol for the assessment of material behavior under UV-C radiation is defined by the Business and Institutional Furniture Manufacturers Association (BIFMA, Grand Rapids, MI, USA) [60]. These guidelines were created for healthcare furniture design and specify that materials should be tested with 291 kJ/m^2 of UV-C radiation for a period of 12 to 24 h.

The material analyzed in this study is a copolymer made from ABS (Acrylonitrile Butadiene Styrene) and PC (PolyCarbonate). The tested material is commercially available under the brand name Z-PCABS, manufactured by Zortrax (Olsztyn, Poland). According to the manufacturer, this Z-PCABS blend contains 55–60% ABS, 30–35% PC and up to 10% additives and colorants. The material has a glass transition temperature of 104 °C and melts at a temperature of 260 °C (manufacturer specifications). The rated tensile strength is 36.89 MPa (ISO 527:1998 [61]), and the material's specific density is 1.14 g/cm^3. The material was sourced as a 1 kg spool of 1.75 mm diameter filament, opaque, ivory color. The spool of material was provided in a sealed reflective bag that included silica desiccant and was unsealed only prior to printing. Decisive in material selection was the fact that many filament manufacturers have settled on this composition based on process-specific requirements. When used for 3D printing, ABS should be extruded at temperatures between 230 °C and 260 °C while PC requires a higher temperature, 260 °C to 300 °C. As PC content in the blend increases, so does the temperature needed to process the material. The selected ABS/PC ratio places this material at the upper end of what common 3D printers can process in terms of extrusion temperature. Above this temperature, MEX 3D printers need to be equipped with high-temperature resistant components, higher-power ceramic heaters, temperature sensors for high-temperature applications and heated enclosures.

All specimens were 3D printed on a Zortrax M200 3D printer equipped with a 0.4 mm diameter nozzle. Z-Suite software, produced by the same company, was used to section the virtual model into layers. Printing parameters were selected based on what is known to provide consistent printing results [62–65] in order to minimize potential errors related to the manufacturing process. Layer settings used for slicing are layer height = 0.19 mm and layer width = 0.4 mm, with 2 outside perimeters and solid infill using a grid pattern (45° raster angle, alternating each layer [66]). The extrusion temperature was set at 265 °C, and the build platform temperature was set at 85 °C. Parts were printed horizontally [67]. Table 1 shows some of the process parameters used for 3D printing test samples.

Table 1. Main parameters used in the 3D-printing process for sample manufacturing.

Material	Layer Height	Perimeters	Infill	Infill Pattern	Extrusion Temperature	Bed Temperature
Z-PCABS	0.19 mm	2	100%	"Grid" 45°/−45°	265 °C	85 °C

Considering the aspects mentioned above, the 3D-printed test samples (Figure 1a) were subjected to ultraviolet radiation in an Opsytec Dr. Grobel BS-02 irradiation chamber (Ettlingen, Germany) (Figure 1b). The irradiation chamber comes equipped with two

groups of fluorescent lamps, one group emitting UV-C, λ = 254 nm, and the second group emitting UV-B λ = 315 nm. The radiation dose is measured with calibrated sensors and controlled using a UV-MAT controller produced by the same manufacturer [68].

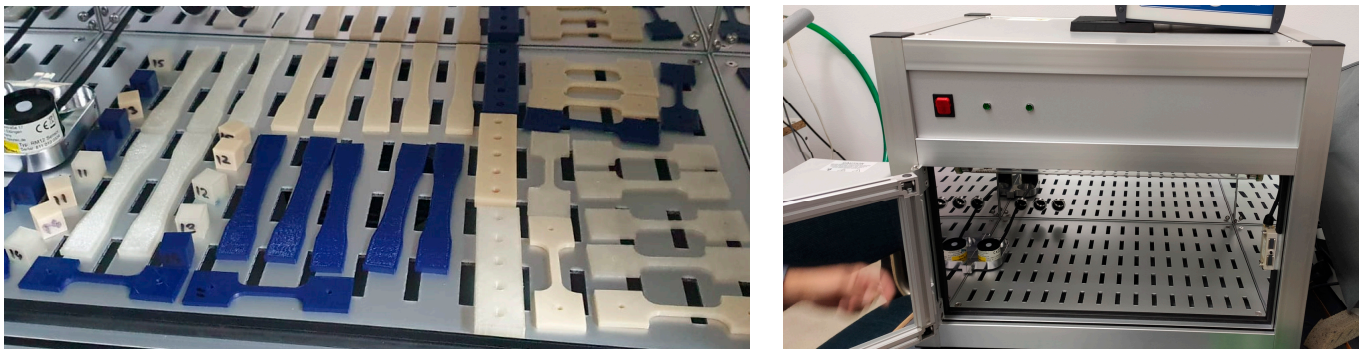

(**a**) (**b**)

Figure 1. Accelerated aging in irradiation chamber (**a**) Test parts positioned for irradiation cycle; (**b**) Irradiation chamber.

A group of 3D-printed samples was exposed to 254 nm radiation for 24 h. During the irradiation cycle, a back panel temperature of 50 °C was maintained in the chamber, and the samples were hit with 10 W/m^2 radiating power. After 24 h, the lamps were turned off, and the test samples were left in the chamber for an additional 4 h to cool down to room temperature. In order to have another reference point for determining radiation effects on the material, a second set of sample parts were exposed to UV-B radiation in the same irradiation chamber.

The effects of UV-B and UV-C radiation were analyzed according to ISO 4892-1:2016, which indicates how data from accelerated aging using light radiation exposure [69] should be analyzed. Tensile and compressive strength tests were designed according to ISO 4582:2017 [70].

For tensile strength determination, 15 specimens were 3D printed from Z-PCABS according to ASTM type I dimensions [71].

For compressive strength tests, 15 test samples measuring 15 mm × 15 mm × 15 mm were 3D printed from the same material.

For each mechanical property test, the samples were split into 3 groups, forming groups of 5 randomly selected samples.

For strength testing (tensile strength, compressive strength), accelerated aging using UV-B radiation using the parameters highlighted previously was performed on the first group of samples. The second group was exposed to UV-C radiation. The third group did not undergo any radiation exposure and represented the control group. Before and after the accelerated aging treatment, all samples were measured using electronic calipers and were visually inspected.

In total, 15 3D-printed samples (dog bone-shaped) were tested for tensile strength on an Instron 8872 machine (Norwood, MA, USA) (Figure 2a). Tests were performed starting with a preload force of 5 N with 1 mm/minute loading speed. Elongation of the test part under tensile load was measured using an electronic extensometer and was used to determine part stiffness. Fifteen 3D-printed cubic samples were tested for compressive strength on an Instron 8801 machine (Norwood, MA, USA) (Figure 2b). The compressive force is applied along the sample Z-axis, perpendicular to the horizontal 3D-printed layers. Preload for this test was 5 N. All strength tests were in controlled conditions of 50% RH at 24 °C.

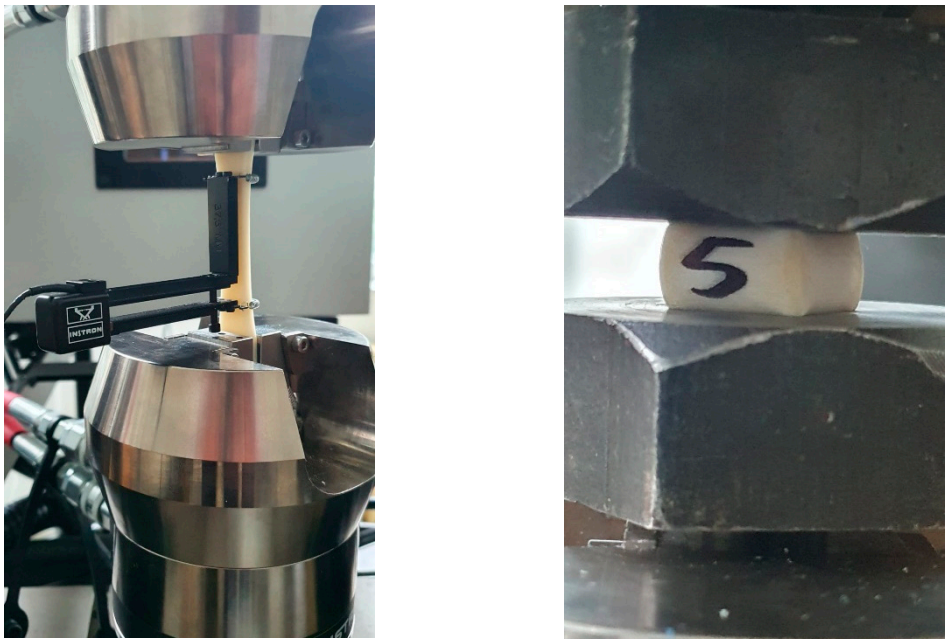

(**a**) (**b**)

Figure 2. Mechanical strength tests: (**a**) Tensile strength testing of 3D printed dog-bone ABS-PC samples; (**b**) Compression strength testing of 3D printed cubic ABS-PC samples.

Section 3.1 details the results of tensile tests (strength, stiffness), while Section 3.2 discusses the results of compressive tests (strength).

Polymers and fibers have a known tendency to deform plastically when subjected to loads for long periods of time, a characteristic commonly referred to as cold flow or creep. For certain polymers, creep-inducing stress can occur even at a small fraction of the material's ultimate strength. ABS-PC blends experience creep, with creep resistance increasing with increased PC content [72,73]. Thus, the effects of radiation on the creep behavior of ABS-PC parts was also investigated. Tensile creep testing was performed on 10 3D-printed specimens with a narrow section of 5.2 mm × 3 mm (Figure 3a). Testing was performed in compliance with standard ASTM D2990-17 [74]. The creep behavior of parts exposed to UV-C radiation was compared to that of parts in a control group.

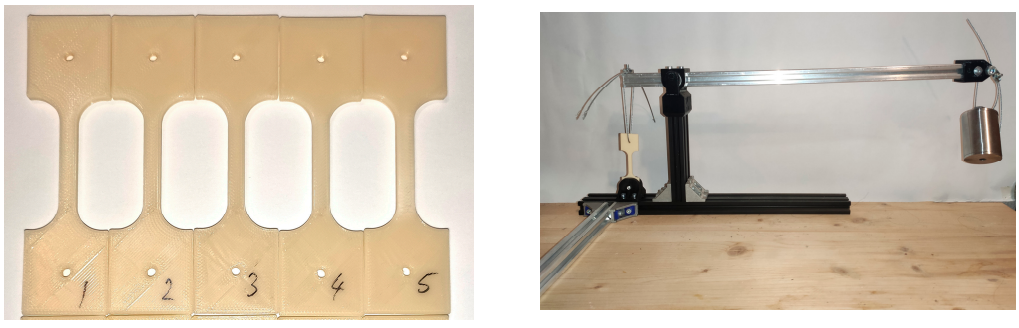

(**a**) (**b**)

Figure 3. Creep properties testing: (**a**) 3D printed parts made for tension creep testing; (**b**) Testing rig for determining tensile creep.

For finding creep under tensile load, parts were loaded in tension in a purposefully designed rig (Figure 3b). Creep was determined by applying a load that produces mechanical stress of 25% of the ultimate tensile strength measured previously for parts in the control group. Sample elongation under this tensile load was measured after 2 h, 6 h, 21 h, 24 h, then once every 24 h for a total of 168 h (7 days). The distance between the ends of the

samples was measured using a micrometer on each side of the narrow section (left and right sides). The average change in these two distances was considered as elongation. The results of creep testing are discussed in Section 3.3.

The exterior surfaces and internal structure of the samples were analyzed using Scanning Electron Microscopy analysis (SEM). One sample each was selected from the group exposed to 254 nm radiation and from the control group. The analysis was performed using a Quanta Inspect F50 scanning electron microscope from Thermo Fisher Scientific (Eindhoven, The Netherlands) at a resolution of 1.2 nm. A layer of Au was sputter-coated on the samples (coverage time 90 s) using a Quorum Technologies Q150 PlusSeries coater (Lewes, UK). Section 3.4 discusses SEM results.

3. Results

Dimensional and visual checks were performed on the parts before and after accelerated aging under 254 nm radiation. Dimensions of the UV-C exposed parts were measured using electronic calipers before and after irradiation, revealing no statistically relevant changes in dimensions after UV-C exposure. Table 2 shows the average dimensions of samples in the aged group vs. the control group.

Table 2. Sample dimensions were measured using electronic calipers.

	Tensile Strength Sample		Compression Strength Sample	
	Width	**Height**	**X**	**Z**
3D model [mm]	13.00	4.20	15.00	15.00
Control samples [mm]	13.07 ± 0.012	4.15 ± 0.016	15.00 ± 0.016	15.16 ± 0.010
UV-C samples [mm]	13.09 ± 0.010	4.14 ± 0.010	15.01 ± 0.010	15.18 ± 0.012

3.1. Tensile Strength and Young's Modulus

Visual analysis of the failure mechanism found that the ABS-PC samples fractured along the deposited polymer filaments, creating a zig-zag failure pattern. The same pattern was observed in the control group and both groups exposed to radiation (UV-B/UV-C) (Figure 4). This fracture pattern can be explained by considering the anisotropic mechanical properties of parts produced through MEX 3D printing [75]. The anisotropy is caused by higher tensile strength along the filaments than the tensile strength of the adhesion between adjacent filaments [76] and is influenced by print orientation, infill type and amount, raster angle, and layer height [77–79]. The similar failure modes for all tested groups also indicate that changes generated by the irradiation treatments were uniform throughout the parts. The parts displayed a slight browning of the ivory-colored material following irradiation. A similar amount of browning is found in both UV-B and UV-C groups.

(**a**) (**b**) (**c**)

Figure 4. Fracture modes of tensile-tested parts: (**a**) Fractured ABS-PC parts from the control group; (**b**) Fractured ABS-PC parts exposed to UV-B; (**c**) Fractured ABS-PC parts exposed to UV-C.

Experimental data from tensile testing of PC-ABS are shown in Figure 5 as stress-strain graphs.

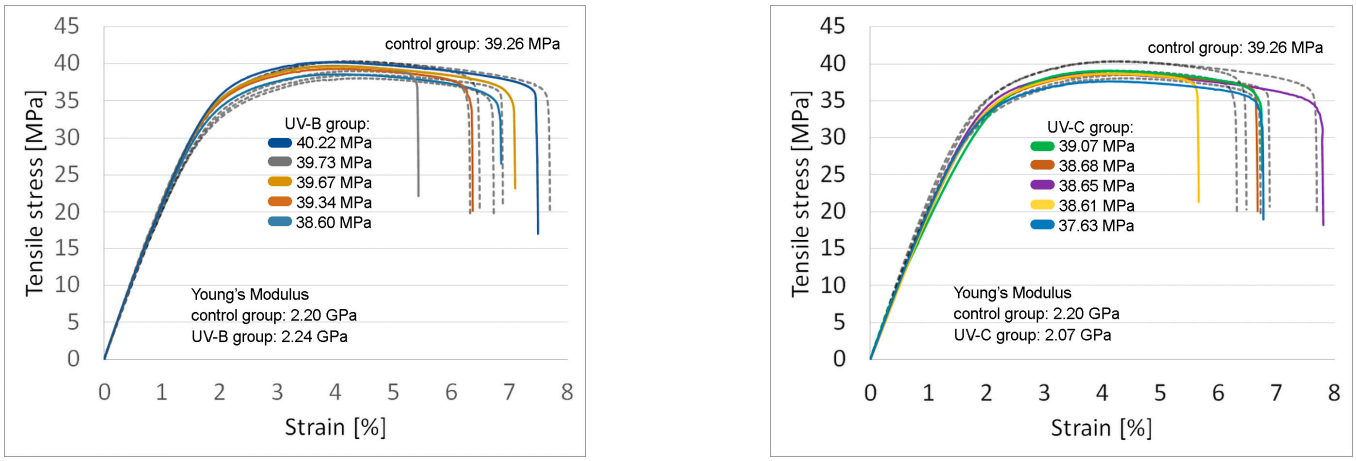

Figure 5. Stress-strain diagrams (tensile tests): (**a**) Samples exposed to UV-B λ = 315 nm (solid line) and samples from the control group (dashed line); (**b**) Samples exposed to UV-C λ = 254 nm (solid line) and samples from the control group (dashed line).

Dog bone-shaped samples made from ABS-PC subjected to the previously described dose of UV-B radiation had no statistically significant difference in tensile strength (39.51 MPa vs. 39.26 MPa; $F = 0.23$, $p = 0.65$) and stiffness (2238.06 MPa vs. 2196 MPa; $F = 1.57$, $p = 0.24$) compared to the parts in the control group.

Parts made from ABS-PC aged under UV-C exhibited 1.86% lower tensile strength compared to control samples (38.53 MPa vs. 39.26 MPa), a result that is not statistically significant ($F = 1.91$, $p = 0.20$). On average, the Young's Modulus of aged samples decreased by 5.51% vs. control samples (2075 MPa vs. 2196 MPa), a result that was determined to be statistically significant ($F = 5.70$, $p = 0.04$).

Results for average tensile strength after calculating the standard error can be found in Table 3. The same table shows the average Young's Modulus.

Table 3. Experimental results—average tensile strength and Young's Modulus.

Property	ABS-PC (no UV)	ABS-PC (UV-B)	ABS-PC (UV-C)
Tensile strength [MPa]	39.26 ± 0.47	39.51 ± 0.27	38.53 ± 0.24
Young's Modulus [MPa]	2196.4 ± 31.7	2238.1 ± 9.78	2074.9 ± 39.8

3.2. Compressive Strength

Compressive loads applied during compressive strength testing deformed the parts plastically without visible material rupture at their surface. Compared to parts in the control group (no UV exposure), all samples in the accelerated aging groups performed worse. Overall, ABS-PC samples have 5.2% lower compressive strength after UV-B irradiation (58.60 MPa vs. 61.81 MPa; $F = 33.8$, $p = 4 \times 10^{-4}$) while samples subjected to UV-C radiation have 6.5% lower compressive strength than those in the control group (57.82 MPa vs. 61.81 MPa; $F = 36.3$, $p = 3 \times 10^{-4}$). Stress-strain diagrams for ABS-PC are shown in Figure 6.

Results for average compressive strength after calculating standard error are shown in Table 4.

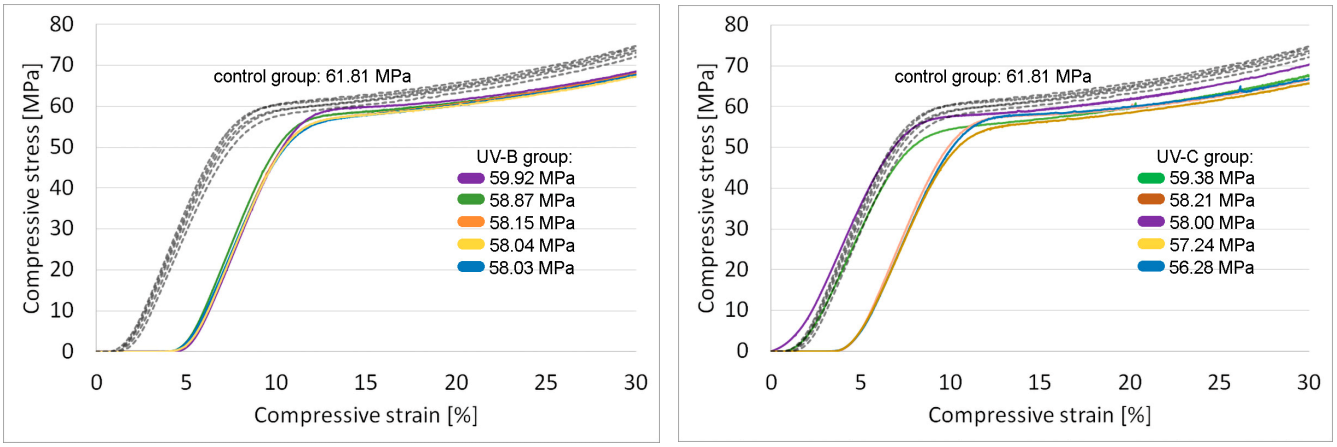

(**a**) (**b**)

Figure 6. Stress-strain diagrams (compressive tests): (**a**) ABS-PC samples exposed to UV-B λ = 315 nm (solid line) and control samples (dashed line); (**b**) ABS-PC samples exposed to UV-C λ = 254 nm (solid line) and control samples (dashed line).

Table 4. Experimental results—average compressive strength.

Property	ABS-PC (no UV)	ABS-PC (UV-B)	ABS-PC (UV-C)
Compressive str. [MPa]	61.81 ± 0.41	58.60 ± 0.37	57.82 ± 0.52

3.3. Creep Characteristics of the Analyzed Material

Tensile creep testing was performed with loads appropriate to the tested material based on the tensile strength value identified previously ($\sigma_{Z\text{-}PCABS}$ = 39.26 MPa). The parts are placed in a testing rig that uses mechanical advantage to amplify the load applied to one of its ends. The cross-section area of the tested parts is 15.6 mm^2 (5.2 mm × 3 mm). Table 5 shows the main parameters (loads) used in this experiment.

Table 5. Creep testing parameters.

Material	Test Parameter			
	Strength [MPa]	Creep Test Stress [MPa]	Targeted Tensile Force on Sample [N]	Test Rig Load Configuration
ABS-PC	39.26	9.82	154	22 N × 7

Figure 7 shows the tensile creep of ABS-PC samples while being loaded (9.82 MPa) over a period of 168 h. The majority of the elongation took place right after the load was applied, and the rate of creep continued to slow down with the rise in strain. Despite the fact that the parts from the UV-C exposed group experienced more deformation under prolonged tensile stress, they exhibited very similar creep curves.

3.4. Scanning Electron Microscopy (SEM)

To gain insight into how the samples failed under tensile stress and to spot any potential changes in the internal structure following exposure to UV-C radiation, a fractographic analysis was performed using SEM. In Figure 8a, an SEM image is presented, depicting an ABS-PC sample from the control group. Figure 8b displays an SEM image of a sample from the irradiated group (UV-C).

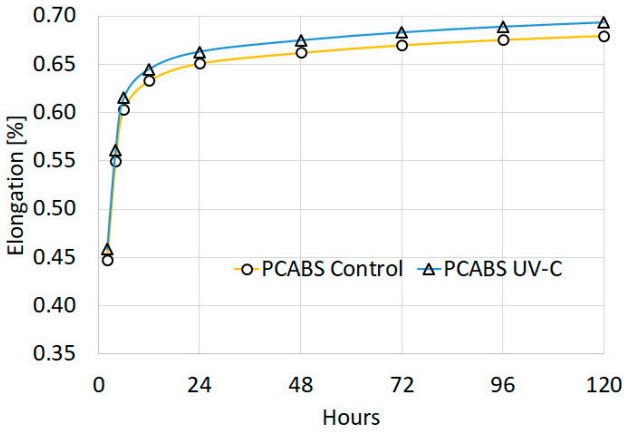

Figure 7. Tensile creep of Z-PCABS; graph showing an increase in elongation over time.

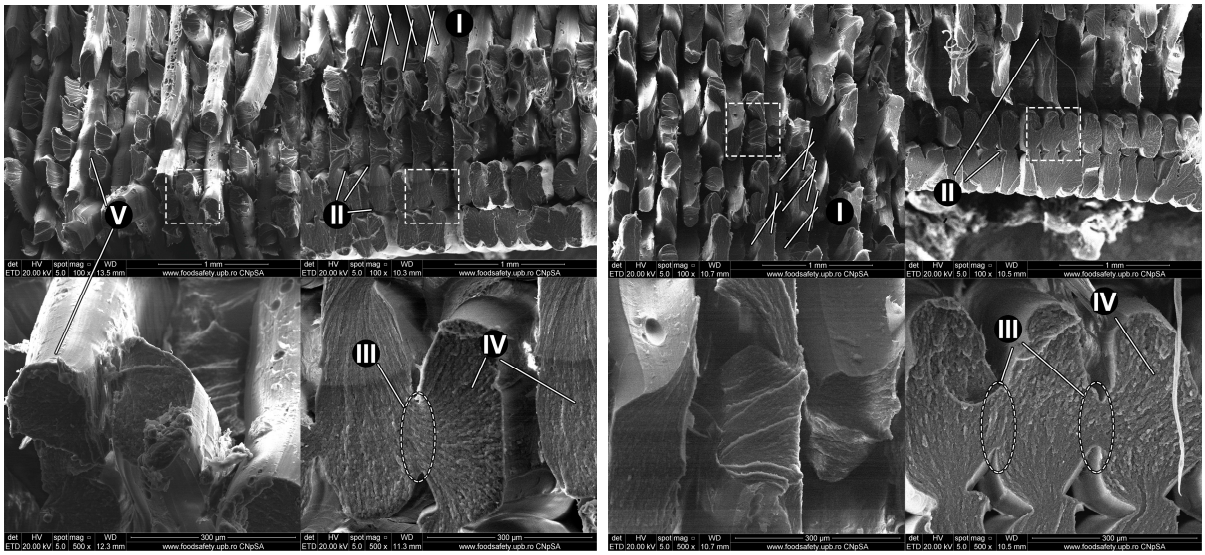

(**a**) (**b**)

Figure 8. SEM imaging of fractured ABS-PC sample with the left column showing rupture surfaces in part infill; right column showing rupture surface in part contour: (**a**) Z-PCABS sample from the control group; (**b**) Z-PCABS sample exposed to UV-C λ = 254 nm; I—fracture parallel with filaments; II—microvoids; III—interlayer fusion; IV—extensive flaking at the fractured surface; V—reduced necking of the ruptured filaments.

The ABS-PC samples fractured along the deposited filament lines (Figure 8a,b-I), as previously described in Section 3.1. Overlap of the deposited filaments, along with flattening following deposition, can be observed, giving the filaments a characteristic oblong shape. The MEX process introduces in the manufactured parts specific gaps usually referred to as "microvoids". These voids are triangular in shape due to the angled raster used with infill deposition and the oblong shape of deposited filaments and form weak points in the material structure [80]. The formation of microvoids is generally associated with the lack of pressure applied to the molten filament while it is being deposited, unlike other manufacturing processes, such as injection molding [81]. Microvoids can be observed in both SEM-analyzed samples, with or without radiation exposure (Figure 8a,b-II).

Interlayer adhesion is distinctly noticeable in both the control sample (Figure 8a-III) and the radiation-aged sample (Figure 8b-III). Samples from both groups present flaking at the rupture surface with small areas of smooth fracture surface (Figure 8a,b-IV), with the control part also showing reduced necking of ruptured filaments (Figure 8a-V). This indicates the parts do not display increased brittleness after 24 h of UV-C exposure.

4. Discussion

This work investigated how sterilizing UV-C radiation λ = 254 nm affects the mechanical properties of ABS-PC components after 24 h of exposure. This is particularly significant when considering the growing use of 3D printing for functional parts. The study evaluated the tensile and compressive strength of samples that were 3D printed using the same process parameters and then exposed to 2 different radiation wavelengths (UV-B λ = 315 nm, UV-C λ = 254 nm). The group of parts exposed to a UV-C accelerated aging cycle was compared to a control group.

Following exposure to UV-C radiation ABS-PC parts produced a change in color at their surface, consistent with the degradation of the ABS component [82]. The changes were only visual, with no dimensional differences between parts from both groups. This is true for both bulky parts like the compressive strength tested specimens (15 mm × 15 mm × 15 mm cubes) and for high length-to-width ratio parts like the samples used for tensile strength testing (115 mm × 13 mm dog bone shape).

Laureto et al. [83] found that a difference exists between ASTM D638-14 Type I and Type IV dimensions when testing 3D printed parts, with the type I test specimens producing slightly better results tensile strength results. However, the difference in specimen performance is not expected to influence the conclusions drawn in this paper.

Following tensile strength testing, there was no statistically significant difference between unexposed samples and samples exposed to 24 h of 10 W/m^2. UV-C radiation. A decrease in stiffness was observed after irradiation which can be attributed to the scission of molecular bonds.

Compressive strength testing showed a weakening of ABS-PC following radiation exposure, with aged parts (UV-C) having 6.5% less compressive strength.

Tensile creep testing resulted in similar elongation-time curves for the control group and the irradiated group, mirroring the findings regarding material stiffness. Mohamed et al. found that different printing parameters influence the creep resistance of PC-ABS 3D printed parts [84], a fact that highlights the need for further testing with other parameter sets. The amount of creep and the creep rate should only be associated with the particular use of a $45^\circ/-45^\circ$ infill raster angle. As Zhang et al. have found, the creep resistance of MEX 3D-printed parts is anisotropic and is influenced by infill orientation, with parts printed using 90° infill having the highest creep resistance [85]. However, infill orientation is not expected to produce different relative results (unexposed parts vs UV-C exposed).

SEM imaging was used to investigate whether any changes in the material occurred. Samples from both groups presented features common to the manufacturing process, such as microvoids and interlayer fusion regions. Key aspects commonly used to determine material behavior, such as fracture appearance and fracture surface smoothness, were also similar, mirroring the small differences observed following destructive testing.

UV radiation can cause polymers to age by breaking down their molecular chains, weakening their physical properties. This is because UV radiation contains high-energy photons that are capable of breaking chemical bonds in the polymer chains. When this happens, the polymer molecules become shorter, and the polymer chains become weaker, which can lead to the degradation of the material over time. This process is often referred to as photo-oxidation. One of the primary ways photo-oxidation degrades the material is by initiating the formation of free radicals—highly reactive molecules that can cause chain reactions in the polymer—leading to the formation of new chemical bonds and altering the polymer's structure. In the presence of oxygen, free radicals can also react with oxygen molecules to form peroxides. Peroxides can then react with other polymer molecules to form more free radicals, perpetuating the chain reaction and causing further degradation of the polymer. With short wavelength radiation, such as UV-C, another important effect occurs, namely Fries rearrangement. When high-energy photons are absorbed by the polymer, primarily free radicals can form by breaking carbonate bonds in a process that does not need the presence of oxygen [86].

It is known that PC has better UV resistance compared to non-oxygen polymers, such as ABS [87,88]. We can hypothesize that the good behavior of ABS-PC is not only due to the PC component being more UV resistant, but its presence could aid the ABS component as well. It is known that at low wavelengths, ultraviolet radiation consists of photons with sufficient energy to break molecular bonds, creating cross-linking and scission effects on polymers [89,90]. It is, thus, possible for the radicals formed in the PC component to have a scavenging effect on other free radicals formed during the cleavage of molecules in the ABS component. This hypothesis requires further investigation.

In addition to causing physical changes in the polymer, UV radiation can also affect its optical properties. Polymers that are exposed to UV radiation can become discolored or yellowed (as was observed in these experiments), as photons can break down chromophores, which are chemical groups responsible for a polymer's color. This is an important aspect to consider when designing parts where functionality depends on the material's optical properties.

A large compilation of 431 studies on the UV dose (fluence) needed to inactivate common pathogens reveals that most pathogens see a 1-log reduction in numbers (90% pathogen inactivation) at UV doses lower than 20 mJ/cm^2 [91,92]. This is equivalent to 20 s of exposure to the UV-C radiation source used in this experiment. These factors indicate that the investigated aging treatment is relevant to the common practices of sterilizing materials and surfaces. Given the good response of ABS-PC 3D-printed parts in terms of tensile and compressive strength, stiffness and creep behavior before and after UV exposure, this material should be considered for applications where UV sterilizing is employed. This study looked at the performance of a common commercially available ABS-PC blend. As discussed previously, a higher ratio of PC would increase UV stability while decreasing processability through MEX 3D printing. Further improvement of the material's performance and stability under ultraviolet radiation could be obtained through various methods. Additives, such as organo-modified layered double hydroxides are known to increase the photostability of polymers while providing anti-bacterial properties [93]. Other UV absorbers and UV stabilizers can also be used [94]. Another aspect worth studying is the replacement of ABS with acrylonitrile styrene acrylate (ASA) in a PC/ASA copolymer. ASA has superior UV resistance compared to ABS, but a PC/ASA copolymer requires higher processing temperatures (275 °C extrusion temperature, 110 °C bed temperature). It is important to note that the presence of MEX process-specific features, such as layer lines, microvoids, etc., may play a role in determining the sterilization efficiency of 3D-printed parts, and future studies need to address this fact.

5. Conclusions

The objective of this paper was to examine the impact of UV-C exposure-induced accelerated aging on the mechanical characteristics of ABS-PC copolymer samples manufactured through MEX 3D printing. Mechanical testing found minor tensile and compressive strength decreases following irradiation. The same tests found that UV-C radiation has slightly decreased part stiffness.

After conducting a tensile creep test, it was observed that the creep behavior remained unchanged even after exposure to UV-C radiation, and both exposed and unexposed materials exhibited comparable creep curves.

The results overall suggest a minor reduction in mechanical properties of 3D printed ABS-PC parts following an irradiation treatment. These minor changes in mechanical properties, coupled with the proven long-term stability of ABS-PC blends, suggest that these materials are suitable for use in the presented scenarios. This is also true for parts subjected to continuous tensile stress and vulnerable to polymer creep. SEM investigation mirrored the findings of destructive testing,

Testing is needed to assess the medical efficiency of ultraviolet UV-C sterilization on such parts, given the inherent characteristics of MEX 3D printed materials. Elements,

such as surface porosity, hygroscopy, etc., may represent a hurdle in the adoption of these materials.

It is important to mention that variations in feedstock material compositions, 3D printing equipment and software, and different printing parameters may yield slightly different outcomes for MEX 3D printed parts, as emphasized by Popescu et al. in a review of mechanical property testing [95]. In-house assessment of material properties, 3D-printing machine characteristics and parameter sets is recommended before producing end-use polymer parts.

Author Contributions: Conceived the experiments, A.Z. and C.G.A.; performed the experiments, A.Z., F.B. and C.R.; analyzed the data obtained from the 3D prints, A.Z., F.B. and C.G.A. All authors have read and agreed to the published version of the manuscript.

Funding: This research received no external funding.

Institutional Review Board Statement: Not applicable.

Informed Consent Statement: Not applicable.

Data Availability Statement: Data will be made available on request.

Conflicts of Interest: The authors declare no conflict of interest. The funders had no role in the design of the study; in the collection, analyses, or interpretation of data; in the writing of the manuscript, or in the decision to publish the results.

References

1. World Health Organization. Shortage of Personal Protective Equipment Endangering Health Workers Worldwide. 2020. Available online: https://www.who.int/news/item/03-03-2020-shortage-of-personal-protective-equipment-endangering-health-workers-worldwide. (accessed on 15 March 2023).
2. Blanco-Donoso, L.M.; Moreno-Jiménez, J.; Amutio, A.; Gallego-Alberto, L.; Moreno-Jiménez, B.; Garrosa, E. Stressors, job re-sources, fear of contagion, and secondary traumatic stress among nursing home workers in face of the COVID-19: The case of Spain. *J. Appl. Gerontol.* **2021**, *40*, 244–256. [CrossRef]
3. Ranney, M.L.; Griffeth, V.; Jha, A.K. Critical Supply Shortages—The Need for Ventilators and Personal Protective Equipment during the COVID-19 Pandemic. *N. Engl. J. Med.* **2020**, *382*, e41. [CrossRef] [PubMed]
4. Webber, L.; Jewett, C. Testing Swabs Run in Short Supply as Makers Try to Speed up Production. Available online: https://www.npr.org/sections/health-shots/2020/03/18/817801222/testing-swabs-run-in-short-supply-as-makers-try-to-speed-up-production (accessed on 18 March 2023).
5. Hufford, A. 3M CEO on N95 Masks: 'Demand Exceeds Our Production Capacity'. 2020. Available online: https://www.wsj.com/articles/3m-ceo-on-n95-masks-demand-exceeds-our-production-capacity-11585842928 (accessed on 20 March 2023).
6. Chen, P.G.; Chan, E.W.; Qureshi, N.; Shelton, S.; Mulcahy, A.W. RAND Health Care–Project Report. Medical Device Supply Chains An Overview and Description of Challenges During the COVID-19 Pandemic. 2021. Available online: https://aspe.hhs.gov/sites/default/files/documents/e48047020834c0c34cf6baf08a9428d0/PR-A328-2-medicaldevices.pdf (accessed on 20 March 2023).
7. Park, C.-Y.; Kim, K.; Roth, S.; Beck, S.; Kang, J.W.; Tayag, M.C.; Griffin, M. Global Shortage of Personal Protective Equipment amid COVID-19: Supply Chains, Bottlenecks, and Policy Implications. *ADB Briefs* **2020**, 130. [CrossRef]
8. Bown, C.P. How COVID-19 Medical Supply Shortages Led to Extraordinary Trade and Industrial Policy. *Asian Econ. Policy Rev.* **2022**, *17*, 114–135. [CrossRef]
9. Ibn-Mohammed, T.; Mustapha, K.B.; Godsell, J.; Adamu, Z.; Babatunde, K.A.; Akintade, D.D.; Acquaye, A.; Fujii, H.; Ndiaye, M.M.; Yamoah, F.A.; et al. A critical analysis of the impacts of COVID-19 on the global economy and ecosystems and opportunities for circular economy strategies. *Resour. Conserv. Recycl.* **2021**, *164*, 105169. [CrossRef] [PubMed]
10. Cohen, J.; Rodgers, Y. Contributing factors to personal protective equipment shortages during the COVID-19 pandemic. *Prev. Med.* **2020**, *141*, 106263. [CrossRef] [PubMed]
11. Jordan, J.M. Additive manufacturing ("3D printing") and the future of organizational design: Some early notes from the field. *J. Org. Des.* **2019**, *8*, 5. [CrossRef]
12. Mueller, T.; Elkaseer, A.; Charles, A.; Fauth, J.; Rabsch, D.; Scholz, A.; Marquardt, C.; Nau, K.; Scholz, S.G. Eight Weeks Later—The Unprecedented Rise of 3D Printing during the COVID-19 Pandemic—A Case Study, Lessons Learned, and Implications on the Future of Global Decentralized Manufacturing. *Appl. Sci.* **2020**, *10*, 4135. [CrossRef]
13. Ben-Ner, A.; Siemsen, E. Decentralization and Localization of Production: The Organizational and Economic Consequences of Additive Manufacturing (3D Printing). *Calif. Manag. Rev.* **2017**, *59*, 000812561769528. [CrossRef]
14. Malik, A.; Ul Haq, M.I.; Raina, A.; Gupta, K. 3D printing towards implementing Industry 4.0: Sustainability aspects, barriers and challenges. *Ind. Rob.* **2022**, *49*, 491–511. [CrossRef]

15. Choong, Y.Y.C.; Tan, H.W.; Patel, D.C.; Choong, W.T.N.; Chen, C.-H.; Low, H.Y.; Tan, M.J.; Patel, C.D.; Chua, C.K. The global rise of 3D printing during the COVID-19 pandemic. *Nat. Rev. Mater.* **2020**, *5*, 637–639. [CrossRef]
16. Maracaja, L.; Blitz, D.; Maracaja, D.; Walker, C. How 3D Printing Can Prevent Spread of COVID-19 Among Healthcare Professionals During Times of Critical Shortage of Protective Personal Equipment. *J. Cardiothorac. Vasc. Anesth.* **2020**, *34*, 2847–2849. [CrossRef]
17. Manero, A.; Smith, P.; Koontz, A.; Dombrowski, M.; Sparkman, J.; Courbin, D.; Chi, A. Leveraging 3D Printing Capacity in Times of Crisis: Recommendations for COVID-19 Distributed Manufacturing for Medical Equipment Rapid Response. *Int. J. Environ. Res. Public Health* **2020**, *17*, 4634. [CrossRef] [PubMed]
18. Hagen, A.; Chisling, M.; House, K.; Katz, T.; Abelseth, L.; Fraser, I.; Bradley, S.; Kirsch, R.; Morris, J.; Giles, J.W.; et al. 3D Printing for Medical Applications: Current State of the Art and Perspectives during the COVID-19 Crisis. *Surgeries* **2021**, *2*, 244–259. [CrossRef]
19. Longhitano, G.A.; Nunes, G.B.; Candido, G.; da Silva, J.V.L. The role of 3D printing during COVID-19 pandemic: A review. *Prog. Addit. Manuf.* **2021**, *6*, 19–37. [CrossRef]
20. Radfar, P.; Bazaz, S.R.; Mirakhorli, F.; Warkiani, M.E. The role of 3D printing in the fight against COVID-19 outbreak. *J. 3D Print. Med.* **2021**, *5*, 51–60. [CrossRef]
21. Ford, J.; Goldstein, T.; Trahan, S.; Neuwirth, A.; Tatoris, K.; Decker, S. A 3D-printed nasopharyngeal swab for COVID-19 diagnostic testing. *3D Print. Med.* **2020**, *6*, 21. [CrossRef]
22. Alyouha, S.; Almazeedi, S.; Alghounaim, M.; Al-Mutawa, Y.; Alsabah, S. Polyester tipped 3-dimensionally printed swab that costs less than US$0.05 and can easily and rapidly be mass produced. *BMJ Innov.* **2020**, *6*, 262–264. [CrossRef]
23. Manoj, A.; Bhuyan, M.; Banik, S.R.; Sankard, M.R. 3D printing of nasopharyngeal swabs for COVID-19 diagnose: Past and current trends. *Mater. Today Proc.* **2021**, *44*, 1361–1368. [CrossRef]
24. Wesemann, C.; Pieralli, S.; Fretwurst, T.; Nold, J.; Nelson, K.; Schmelzeisen, R.; Hellwig, E.; Spies, B.C. 3-D Printed Protective Equipment during COVID-19 Pandemic. *Materials* **2020**, *13*, 1997. [CrossRef]
25. Novak, J.I.; Loy, J. A quantitative analysis of 3D printed face shields and masks during COVID-19. *Emerald Open Research* **2020**, *2*, 42. [CrossRef]
26. Wong, K.V.; Hernandez, A. A Review of Additive Manufacturing. *Int. Sch. Res. Not.* **2012**, *2012*, 208760. [CrossRef]
27. Ju, J.; Boisvert, L.N.; Zuo, Y.Y. Face masks against COVID-19: Standards, efficacy, testing and decontamination methods. *Adv. Colloid Interface Sci.* **2021**, *292*, 102435. [CrossRef]
28. O'Kelly, E.; Arora, A.; Pirog, S.; Ward, J.; Clarkson, P.J. Comparing the fit of N95, KN95, surgical, and cloth face masks and assessing the accuracy of fit checking. *PLoS ONE* **2021**, *16*, e0245688. [CrossRef]
29. Dugdale, C.M.; Walensky, R.P. Filtration Efficiency, Effectiveness, and Availability of N95 Face Masks for COVID-19 Prevention. *JAMA Intern. Med.* **2020**, *180*, 1612–1613. [CrossRef]
30. Ballard, D.H.; Jammalamadaka, U.; Meacham, K.W.; Hoegger, M.J.; Burke, B.A.; Morris, J.A.; Scott, A.R.; O'Connor, Z.; Gan, C.; Hu, J.; et al. Quantitative Fit Tested N95 Respirator-Alternatives Generated with CT Imaging and 3D Printing: A Response to Potential Shortages During the COVID-19 Pandemic. *Acad. Radiol.* **2021**, *28*, 158–165. [CrossRef] [PubMed]
31. McAvoy, M.; Bui, A.T.N.; Hansen, C.; Plana, D.; Said, J.T.; Yu, Z.; Yang, H.; Freake, J.; Van, C.; Krikorian, D.; et al. 3D Printed frames to enable reuse and improve the fit of N95 and KN95 respirators. *BMC Biomed. Eng.* **2021**, *3*, 10. [CrossRef] [PubMed]
32. Tipnis, N.P.; Burgess, D.J. Sterilization of implantable polymer-based medical devices: A review. *Int. J. Pharm.* **2018**, *544*, 455–460. [CrossRef] [PubMed]
33. Ghobeira, R.; Philips, C.; Declercq, H.; Cools, P.; De Geyter, N.; Cornelissen, R.; Morent, R. Effects of different sterilization methods on the physico-chemical and bioresponsive properties of plasma-treated polycaprolactone films. *Biomed. Mater.* **2017**, *12*, 015017. [CrossRef] [PubMed]
34. Holmes, S. An overview of current surgical instrument and other medical device decontamination practices. In *Woodhead Publishing Series in Biomaterials, Decontamination in Hospitals and Healthcare*, 2nd ed.; Walker, J., Ed.; Woodhead Publishing: Sawston, UK, 2020; pp. 443–482. [CrossRef]
35. Sadeque, M.; Balachandran, S.K. Overview of medical device processing. In *Trends in Development of Medical Devices*; Shanmugam, P.S.T., Chokkalingam, L., Bakthavachalam, P., Eds.; Academic Press: Cambridge, MA, USA, 2020; pp. 177–188. [CrossRef]
36. McEvoy, B.; Rowan, N. Terminal sterilization of medical devices using vaporized hydrogen peroxide: A review of current methods and emerging opportunities. *J. Appl. Microbiol.* **2019**, *127*, 1403–1420. [CrossRef] [PubMed]
37. Popescu, D.; Baciu, F.; Vlasceanu, D.; Cotrut, M.C.; Marinescu, R. Effects of multiple sterilizations and natural aging on the mechanical behavior of 3D-printed ABS. *Mech. Mater.* **2020**, *148*, 103423. [CrossRef]
38. Grzelak, K.; Łaszcz, J.; Polkowski, J.; Mastalski, P.; Kluczyński, J.; Łuszczek, J.; Torzewski, J.; Szachogłuchowicz, I.; Szymaniuk, R. Additive Manufacturing of Plastics Used for Protection against COVID19—The Influence of Chemical Disinfection by Alcohol on the Properties of ABS and PETG Polymers. *Materials* **2021**, *14*, 4823. [CrossRef] [PubMed]
39. Popescu, D.; Baciu, F.; Amza, C.G.; Cotrut, C.M.; Marinescu, R. The Effect of Disinfectants Absorption and Medical Decontamination on the Mechanical Performance of 3D-Printed ABS Parts. *Polymers* **2021**, *13*, 4249. [CrossRef] [PubMed]
40. Lindsley, W.G.; Martin, S.B., Jr.; Thewlis, R.E.; Sarkisian, K.; Nwoko, J.O.; Mead, K.R.; Noti, J.D. Effects of Ultraviolet Germicidal Irradiation (UVG) on N95 Respirator Filtration Performance and Structural Integrity. *J. Occup. Environ. Hyg.* **2015**, *12*, 509–517. [CrossRef]

41. van Doremalen, N.; Bushmaker, T.; Morris, D.H. Letter to the Editor: Aerosol and Surface Stability of HCoV-19 (SARS-CoV-2) Compared to SARS-CoV-1. *N. Engl. J. Med.* **2020**, *382*, 1564–1567. [CrossRef]
42. Stojalowski, P.S.; Fairfoull, J. Comparison of Reflective Properties of Materials Exposed to Ultraviolet-C Radiation. *J. Res. Natl. Inst. Stand. Technol.* **2021**, *126*, 126017. [CrossRef]
43. Spicer, D.B. Methods and Mechanisms of Photonic Disinfection. *J. Res. Natl. Inst. Stand. Technol.* **2021**, *126*, 126016. [CrossRef]
44. *Standard ISO 4892-3:2016*; Plastics–Methods of Exposure to Laboratory Light Sources–Part 3: Fluorescent UV Lamps. Available online: https://www.iso.org/standard/67793.html (accessed on 25 March 2023).
45. The National Institute of Standards and Technology. Summary of Event and Post-Workshop Activities. 2020. Available online: https://www.nist.gov/news-events/events/2020/01/workshop-ultraviolet-disinfection-technologies-healthcare-associated-4 (accessed on 25 March 2023).
46. IUVA Fact Sheet on UV Disinfection for COVID-19. Available online: https://www.iuva.org/IUVA-Fact-Sheet-on-UV-Disinfection-for-COVID-19 (accessed on 25 March 2023).
47. Ngo, T.D.; Kashani, A.; Imbalanzo, G.; Nguyen, K.; Hui, D. Additive manufacturing (3D printing): A review of materials, methods, applications and challenges. *Comp. Part B Eng.* **2018**, *143*, 172–196. [CrossRef]
48. Cantrell, J.; Rohde, S.; Damiani, D.; Gurnani, R.; DiSandro, L.; Anton, J.; Young, A.; Jerez, A.; Steinbach, D.; Kroese, C.; et al. Experimental Characterization of the Mechanical Properties of 3D-Printed ABS and Polycarbonate Parts. In *Advancement of Optical Methods in Experimental Mechanics*; Yoshida, S., Lamberti, L., Sciammarella, C., Eds.; Conference Proceedings of the Society for Experimental Mechanics Series; Springer: Cham, Switzerland, 2016; Volume 3. [CrossRef]
49. Arivazhagan, A.; Masood, S.H. Dynamic mechanical properties of ABS material processed by fused deposition modelling. *Int. J. Eng. Res. Appl. (IJERA)* **2012**, *2*, 2009–2014.
50. Pérez, J.; Vilas, J.; Laza, J.; Arnaiz, S.; Mijangos, F.; Bilbao, E.; León, L. Effect of Reprocessing and Accelerated Weathering on ABS Properties. *J. Environ. Polym. Degrad.* **2010**, *18*, 71–78. [CrossRef]
51. Li, J.; Chen, F.; Yang, L.; Jiang, L.; Dan, Y. FTIR analysis on aging characteristics of ABS/PC blend under UV-irradiation in air. *Spectrochim. Acta A Mol. Biomol. Spectrosc.* **2017**, *184*, 361–367. [CrossRef]
52. Greco, R.; Astarita, M.F.; Dong, L.; Sorrentino, A. Polycarbonate/ABS blends: Processability, thermal properties, and mechanical and impact behavior. *Adv. Polym. Technol.* **1994**, *13*, 259–274. [CrossRef]
53. Suarez, H.; Barlow, W.; Paul, D.R. Mechanical properties of ABS/PC blends. *J. Appl. Polym. Sci.* **1984**, *29*, 3253–3259. [CrossRef]
54. Krache, R.; Debbah, I. Some Mechanical and Thermal Properties of PC/ABS Blends. *Mater. Sci. Appl.* **2011**, *2*, 404–410. [CrossRef]
55. Wildes, G.; Keskkula, H.; Paul, D.R. Fracture characterization of PC/ABS blends: Effect of reactive compatibilization, ABS type and rubber concentration. *Polymer* **1999**, *40*, 7089–7107. [CrossRef]
56. Zortrax Product Page–Z-PCABS. Available online: https://zortrax.com/filaments/z-pcabs/ (accessed on 25 March 2023).
57. U.S. Food & Drug Administration–Discussion Paper: 3D Printing Medical Devices at the Point of Care. 2021. Available online: https://www.fda.gov/medical-devices/3d-printing-medical-devices/3d-printing-medical-devices-point-care-discussion-paper (accessed on 13 April 2023).
58. The Pew Charitable Trusts–Issue Brief: FDA's Regulatory Framework for 3D Printing of Medical Devices at the Point of Care Needs More Clarity. 2022. Available online: https://www.pewtrusts.org/en/research-and-analysis/issue-briefs/2022/07/fdas-regulatory-framework-for-3d-printing-of-medical-devices-needs-more-clarity (accessed on 13 April 2023).
59. *Standard ISO 4892-2:2013*; Plastics—Methods of Exposure to Laboratory Light Sources—Part 2: Xenon-Arc Lamps. Available online: https://www.iso.org/standard/55481.html (accessed on 20 April 2023).
60. *Standard BIFMA HCF 8.1-2014*; Health Care Furniture Design–Guidelines for Cleanability. Business and Institutional Furniture Manufacturers Association: Grand Rapids, MI, USA, 2014.
61. *Standard ISO 527-2*; Plastics—Determination of Tensile Properties—Part 2: Test Conditions for Moulding and Extrusion Plastics. Available online: https://www.iso.org/standard/4593.html (accessed on 20 April 2023).
62. Samykano, M.; Selvamani, S.K.; Kadirgama, K.; Ngui, W.K.; Kanagaraj, G.; Sudhakar, K. Mechanical property of FDM printed ABS: Influence of printing parameters. *Int. J. Adv. Manuf. Technol.* **2019**, *12*, 2779–2796. [CrossRef]
63. Vicente, C.M.; Martins, T.S.; Leite, M.; Ribeiro, A.; Reis, L. Influence of fused deposition modeling parameters on the mechanical properties of ABS parts. *Polym. Adv. Technol.* **2020**, *31*, 501–507. [CrossRef]
64. Giannatsis, J.; Sofos, K.; Canellidis, V.; Karalekas, D.; Dedoussis, V. Investigating the influence of build parameters on the mechanical properties of FDM parts. In *Innovative Developments in Virtual and Physical Prototyping, Proceedings of the 5th International Conference on Advanced Research and Rapid Prototyping, Leiria, Portugal, 28 September—1 October 2011*; Taylor & Francis: Abingdon, UK, 2012; pp. 525–529.
65. Tymrak, B.M.; Kreiger, M.; Pearce, J.M. Mechanical properties of components fabricated with open-source 3-D printers under realistic environmental conditions. *Mater. Des.* **2014**, *58*, 242–246. [CrossRef]
66. Galeja, M.; Hejna, A.; Kosmela, P.; Kulawik, A. Static and Dynamic Mechanical Properties of 3D Printed ABS as a Function of Raster Angle. *Materials* **2020**, *13*, 297. [CrossRef] [PubMed]
67. Górski, F.; Wichniarek, R.; Kuczko, W.; Zawadzki, P.; Buń, P. Strength of ABS parts produced by Fused Deposition Modelling technology–a critical orientation problem. *Adv. Sci. Technol.* **2015**, *9*, 12–19. [CrossRef]
68. Opsytec Dr. Grobel. Product Datasheet-Irradiation Chamber BS-02. Available online: https://www.opsytec.com/fileadmin/user_upload/products/downloads/e_bs02.pdf. (accessed on 11 April 2023).

69. *Standard ISO 4892-1:2016*; Plastics—Methods of Exposure to Laboratory Light Sources—Part 1: General Guidance. Available online: https://www.iso.org/standard/60048.html (accessed on 20 March 2023).
70. *Standard ISO 4582:2017*; Plastics—Determination of Changes in Colour and Variations in Properties after Exposure to Glass-Filtered Solar Radiation, Natural Weathering or Laboratory Radiation Sources. Available online: https://www.iso.org/standard/67791.html (accessed on 20 March 2023).
71. *Standard ASTM D638–22*; Standard Test Method for Tensile Properties of Plastics. Available online: https://www.astm.org/Standards/D638 (accessed on 25 March 2023).
72. Hassan, A.; Jwu, W.Y. Mechanical properties of high impact ABS/PC blends–effect of blend ratio. In Proceedings of the Polymer Symposium, Kebangsaan Ke-V, Selangor, Malaysia, 23–24 August 2005; pp. 65–76.
73. Bano, S.; Iqbal, T.; Ramzan, N.; Farooq, U. Study of Surface Mechanical Characteristics of ABS/PC Blends Using Nanoindentation. *Processes* **2021**, *9*, 637. [CrossRef]
74. *Standard ASTM D2990–17*; Standard Test Methods for Tensile, Compressive, and Flexural Creep and Creep-Rupture of Plastics. Available online: https://www.astm.org/Standards/D2990.htm (accessed on 18 March 2023).
75. Zohdi, N.; Yang, R. Material Anisotropy in Additively Manufactured Polymers and Polymer Composites: A Review. *Polymers* **2021**, *13*, 3368. [CrossRef]
76. Zou, R.; Xia, Y.; Liu, S.; Ping Hu, P.; Hou, W.; Hu, Q.; Shan, C. Isotropic and anisotropic elasticity and yielding of 3D printed material. *Compos. B Eng.* **2016**, *99*, 506–513. [CrossRef]
77. Gordelier, T.J.; Thies, P.R.; Turner, L.; Johanning, L. Optimising the FDM additive manufacturing process to achieve maximum tensile strength: A state-of-the-art review. *Rapid Prototyp. J.* **2019**, *25*, 953–971. [CrossRef]
78. Rajpurohit, S.R.; Dave, H.K. Effect of process parameters on tensile strength of FDM printed PLA parts. *Rapid Prototyp. J.* **2018**, *24*, 1317–1324. [CrossRef]
79. Zhang, J.; Yang, B.; Fu, F.; You, F.; Dong, X.; Dai, M. Resistivity and its anisotropy characterization of 3D-printed acrylonitrile butadiene styrene copolymer (ABS)/carbon black (CB) composites. *Appl. Sci.* **2017**, *7*, 20. [CrossRef]
80. Wickramasinghe, S.; Do, T.; Tran, P. FDM-Based 3D Printing of Polymer and Associated Composite: A Review on Mechanical Properties, Defects and Treatments. *Polymers* **2020**, *12*, 1529. [CrossRef]
81. Dawoud, M.; Taha, I.; Ebeid, S.J. Mechanical behaviour of ABS: An experimental study using FDM and injection moulding techniques. *J. Manuf. Process.* **2016**, *21*, 39–45. [CrossRef]
82. Iannuzzi, G.; Mattsson, B.; Rigdahl, M. Color changes due to thermal ageing and artificial weathering of pigmented and textured ABS. *Polym Eng Sci* **2013**, *53*, 1687–1695. [CrossRef]
83. Laureto, J.; Pearce, J. Anisotropic mechanical property variance between ASTM D638-14 type I and type IV fused filament fabricated specimens. *Polym. Test.* **2018**, *68*, 294–301. [CrossRef]
84. Mohamed, O.A.; Masood, S.H.; Bhowmik, J. Creep Deformation Behaviour of PC-ABS Parts Processed by Fused Deposition Additive Manufacturing under Different Extrusion Parameters. In Proceedings of the Society of Plastics Engineers Conference, SPE ANTECA, Anaheim, CA, USA, 8–10 May 2017; pp. 13–16.
85. Zhang, H.; Cai, L.; Golub, M.; Zhang, Y.; Yang, X.; Schlarman, K.; Zhang, J. Tensile, Creep, and Fatigue Behaviors of 3D-Printed Acrylonitrile Butadiene Styrene. *J. Materi. Eng. Perform.* **2018**, *27*, 57–62. [CrossRef]
86. Rivaton, A. Recent advances in bisphenol-A polycarbonate photodegradation. *Polym. Degrad. Stab.* **1995**, *49*, 163–179. [CrossRef]
87. Torikai, A.; Mitsuoka, T.; Fueki, K. Wavelength sensitivity of the photoinduced reaction in polycarbonate. *J. Polym. Sci. Part A Polym. Chem.* **1993**, *31*, 2785–2788. [CrossRef]
88. Blakey, I.; Yu, A.; Blinco, J.; Jack, K.S.; Liu, H.; Leeson, M.; Yueh, W.; Younkin, T.; Whittaker, A.K. Polycarbonate Based Nonchemically Amplified Photoresists for Extreme Ultraviolet Lithography. *Extrem. Ultrav. (EUV) Lithogr.* **2010**, *7636*, 952–959. [CrossRef]
89. Ramani, R.; Ranganathaiah, C. Degradation of acrylonitrile-butadiene-styrene and polycarbonate by UV irradiation. *Polym. Degrad. Stab.* **2000**, *69*, 347–354. [CrossRef]
90. Yousif, E.; Haddad, A. Photodegradation and photostabilization of polymers, especially polystyrene: Review. *Springerplus* **2013**, *2*, 398. [CrossRef]
91. Malayeri, A.H.; Mohseni, M.; Cairns, B.; Bolton, J.; Chevrefils, G.; Caron, E. Fluence (UV Dose) Required to Achieve Incremental Log Inactivation of Bacteria, Protozoa, Viruses and Algae, IUVA News. Available online: https://iuva.org/resources/Resource%20Documents/Malayeri-Fluence%20Required%20to%20Achieve%20Incremental%20Log%20Inactivation%20of%20Bacteria,%20Protozoa,%20Viruses%20and%20Algae.pdf (accessed on 25 March 2023).
92. Ledrise Led Professional. Achieving Effective Germicidal Action with UVC Radiation: A Comprehensive Guide. 2021. Available online: https://www.ledrise.eu/blog/uv-fluence-for-disinfection/ (accessed on 25 March 2023).
93. Marek, A.; Verney, V.; Totaro, G.; Sisti, L.; Celli, A.; Bozzi Cionci, N.; Di Gioia, D.; Massacrier, L.; Leroux, F. Organo-modified LDH fillers endowing multi-functionality to bio-based poly(butylene succinate): An extended study from the laboratory to possible market. *Appl. Clay Sci.* **2020**, *188*, 105502. [CrossRef]

94. Rajan, V.; Waber, R.; Wieser, J. Influence of different types of UV absorber/UV stabilizer combination on the photodegradation of PC/ABS blend. *J. Appl. Polym. Sci.* **2011**, *124*, 4007–4015. [CrossRef]
95. Popescu, D.; Zapciu, A.; Amza, C.G.; Baciu, F.; Marinescu, R. FDM process parameters influence over the mechanical properties of polymer specimens: A review. *Polym. Test.* **2018**, *69*, 157–166. [CrossRef]